mater.scichina.com link.springer.com

Published online 15 October 2020 | https://doi.org/10.1007/s40843-020-1443-8
Sci China Mater 2021, 64(3): 642–650

Single-atom Fe with Fe_1N_3 structure showing superior performances for both hydrogenation and transfer hydrogenation of nitrobenzene

Shubo Tian[1†], Min Hu[2†], Qi Xu[1†], Wanbing Gong[3], Wenxing Chen[4], Jiarui Yang[1], Youqi Zhu[4], Chun Chen[3], Jia He[2], Qiang Liu[1], Huijun Zhao[3], Dingsheng Wang[1*] and Yadong Li[1]

ABSTRACT **The design of non-noble metal heterogeneous catalyst with superior performance for selective hydrogenation or transfer hydrogenation of nitroarenes to amines is significant but challenging. Herein, a single-atom Fe supported by nitrogen-doped carbon (Fe_1/N-C) catalyst is reported. The Fe_1/N-C sample shows superior performances for the selective hydrogenation and transfer hydrogenation of nitrobenzene to aniline at different temperatures. Density functional theory (DFT) calculations show that the superior catalytic activity for the selective hydrogenation at lower temperatures could be attributed to the effective activation of the reactant and intermediates by the Fe_1/N-C. Moreover, the excellent performance of Fe_1/N-C for the selective transfer hydrogenation could be attributed to that the reaction energy barrier for dehydrogenation of isopropanol can be overcome by elevated temperatures.**

Keywords: single-atomic Fe catalyst, hydrogenation of nitrobenzene, transfer hydrogenation, DFT calculations

INTRODUCTION

Amines are important chemical intermediates for fine chemicals and pharmaceuticals [1,2]. The selective hydrogenation of nitroarenes to anilines with hydrogen molecules and transfer hydrogenation with organic molecules as the hydrogen donor are extensively utilized approaches in practical applications [3–11]. Although numerous excellent homogeneous catalysts and noble metal heterogeneous catalysts have been developed for the catalytic conversion of nitroarenes to anilines, the difficulties in the separation and reuse of the homogeneous catalysts and the high cost of the noble metal heterogeneous catalysts hinder their further applications [12–15]. Therefore, it remains a significant challenge to synthesize the non-noble metal catalyst that possesses superior performance for the hydrogenation of nitrobenzene. Iron catalyst is one of the most used non-noble metal catalysts in the catalytic reaction, which is the best candidate metal for the hydrogenation of nitrobenzene [16–18]. However, the heterogeneous iron catalyst with excellent catalytic performances for both selective hydrogenation and transfer hydrogenation of nitroarenes has seldom been studied.

Single-atom catalysis has become one of the most active research frontiers in heterogeneous catalysis due to the uniform active site and total atom utilization efficiency [19–36]. The uniform active site can provide an ideal platform for deeper understanding of the fundamentals. Meanwhile, the total atom utilization efficiency can naturally increase the catalytic performance. It is worth noting that the single-atom catalysts have exhibited excellent performances for various reactions. Especially, the

[1] Department of Chemistry, Tsinghua University, Beijing 100084, China
[2] Tianjin Key Laboratory of Advanced Functional Porous Materials; Institute for New Energy Materials & Low-Carbon Technologies, School of Materials Science and Engineering, Tianjin University of Technology, Tianjin 300384, China
[3] Key Laboratory of Materials Physics, Centre for Environmental and Energy Nanomaterials, Anhui Key Laboratory of Nanomaterials and Nanotechnology, Institute of Solid State Physics, Chinese Academy of Sciences, Hefei 230031, China
[4] Beijing Key Laboratory of Construction Tailorable Advanced Functional Materials and Green Applications, School of Materials Science and Engineering, Beijing Institute of Technology, Beijing 100081, China
† These authors contributed equally to this work.
* Corresponding author (email: wangdingsheng@mail.tsinghua.edu.cn)

single-atom Fe catalysts loaded on different supports have shown exceptional catalytic performances for electrocatalysis and selective oxidation [37–43]. However, there are few studies reported the single-atom Fe catalyst with both selective hydrogenation and transfer hydrogenation performance.

Herein, we developed an efficient strategy to synthesize single-atom Fe catalyst anchored on nitrogen-doped carbon (Fe_1/N-C). The as-prepared Fe_1/N-C possessed the Fe_1N_3 structure, which was evidenced by X-ray absorption fine structure (XAFS) data as well as the corresponding fitting and density functional theory (DFT) calculation. The Fe_1/N-C sample showed superior catalytic performances for the selective hydrogenation and transfer hydrogenation of nitrobenzene than the Fe nanoparticles/N-C catalyst. DFT calculation investigated the reaction process and revealed that the reactant could be effectively activated by the Fe_1/N-C at lower temperatures. Furthermore, the energy barrier for dehydrogenation of isopropanol on the Fe_1/N-C could be overcome at higher temperatures.

EXPERIMENTAL SECTION

Materials

Dicyandiamide, dopamine, ammonium hydroxide, and $Fe(acac)_3$ were purchased from Innochem. Nitrobenzene, borane-*tert*-butylamine, and oleylamine were purchased from Aladdin. Ethanol was purchased from Sinopharm Chemical Reagent Co. Ltd. (Shanghai, China). All chemicals were used as received without further purification.

Preparation of the catalysts

Syntheses of g-C_3N_4

Dicyandiamide (10 g) was heated at a rate of 5°C min^{-1} over 2 h to reach a temperature of 600°C and then treated at 600°C for 2 h under flowing N_2 atmosphere. The obtained yellow material was fully grinded to form powder g-C_3N_4.

Syntheses of Fe nanoparticles

$Fe(acac)_3$ (20 mg) was dissolved in 10 mL oleylamine at 250°C under vigorous stirring for about 10 min. Then, a solution of 100 mg borane-*tert*-butylamine in 2 mL oleylamine was added quickly into the above solution. After about 2 min, the flask was then heated to 270°C and then hold at 270°C for 1 h. After cooling to room temperature, the sample was washed three times with ethanol and then dispersed in cyclohexane for future use.

Syntheses of the Fe_1/N-C, Fe nanoparticles/N-C and N-C

The as-prepared g-C_3N_4 (500 mg) and dopamine (500 mg) were dispersed in 100 mL water and 40 mL ethanol mixture solution under ultrasound condition. Ten milliliter of ethanol solution containing 5 mg $Fe(acac)_3$ was added into the above mixture solution under vigorous stirring. After continuous stirring about 10 min, 2 mL ammonium hydroxide was further added. After continuous stirring for about 24 h, the suspension was centrifuged, then washed with H_2O and ethanol, and finally dried under vacuum at room temperature. The resulting powder was heated at a rate of 5°C min^{-1} to reach a temperature of 800°C and then treated at 800°C for 2 h under flowing N_2 atmosphere. The Fe loading is 2.1 wt% determined by inductively coupled plasma optical emission spectroscopy (ICP-OES) analysis. In the same procedure, Fe nanoparticles/N-C were synthesized by changing the $Fe(acac)_3$ to Fe nanoparticles. The Fe loading of Fe nanoparticles/N-C is 5.2 wt% determined by ICP-OES analysis. N-C was synthesized using the same method without adding any Fe species.

Catalytic evaluation

The hydrogenation of nitrobenzene was carried out in a 25-mL stainless steel autoclave with a magnetic stirrer, an automatic temperature control apparatus and a pressure gauge. In a typical experiment, the reaction mixture containing the nitrocompound (1 mmol), catalyst (50 mg Fe_1/N-C, 20 mg Fe NPs/N-C and 50 mg N-C or 50 mg mesoporous g-C_3N_4 (mpg-C_3N_4)) and 5 mL isopropanol were loaded into the reactor. The reactor was sealed, purged two times with N_2 at 1 MPa and then pressurized with 0.5 MPa H_2 and 1 MPa N_2 to a setting point. The reactor was then heated to different temperatures and the stirring speed was fixed to about 1000 r min^{-1}. After 5 h, the autoclave was cooled down to stop the reaction. The products were identified by gas chromatography mass spectrometry and gas chromatography.

The reaction condition for transfer hydrogenation of nitrobenzene was similar with the condition for the hydrogenation of nitrobenzene, expect the atmosphere changed by 1 bar N_2 and without H_2.

During the catalyst stability test, the catalysts were reused without any treatments. More specifically, following the hydrogenation reaction, the reaction mixture was centrifuged to recover the catalyst, which was washed with acetone and then water followed by drying under vacuum oven at 50°C for the next catalytic test.

Characterizations

The X-ray diffraction (XRD) data were recorded on a Rigaku D/max 2500Pc X-ray powder diffractometer. Transmission electron microscopy (TEM) images were recorded on a Hitachi-7700 operated at 100 kV. High-resolution TEM (HRTEM) images were obtained by an FEI Tecnai G2 F20 S-Twin HRTEM working at 200 kV. Aberration-corrected (AC) high-angle annular dark-field scanning TEM (HAADF-STEM) images were imaged by using a Titan 80-300 scanning/transmission electron microscope operated at 300 kV, equipped with a probe spherical aberration corrector. ICP-OES was performed on Thermo Fisher IRIS Intrepid II.

XAFS analysis and results

Fe K-edge X-ray absorption spectra were acquired in fluorescence mode under ambient condition at a 1W1B station in Beijing Synchrotron Radiation Facility (BSRF, operated at 2.5 GeV with a maximum current of 250 mA). All samples were pelletized to disks of 8 mm diameter with 1 mm thickness. The XAFS data were background-subtracted, normalized, and Fourier transformed by standard procedures within the IFEFFIT package. Least-squares curve fitting analysis of the extended XAFS (EXAFS) $\chi(k)$ data was carried out based on the EXAFS equation.

Computational method

All the calculations were carried out using DMol^3 code [44] through spin polarization DFT [45]. The Perdew-Burke-Ernzerhof (PBE) [46] exchange-correlation functional within a generalized gradient approximation was employed. The double numerical plus polarization was chosen as the basis set for other elements. Self-consistent field calculations were performed with a convergence criterion of 2.0×10^{-5}. To ensure high-quality results, the real-space global orbital cut off radius was chosen as high as 4.5 Å. During geometry optimizations, the K-points of Fe (100) is set to be 3×3×1, the K-points of FeN_3 is set to be 5×5×1. Linear synchronous transit/quadratic synchronous transit (LST/QST) method, which has been well validated to find a transition-state structure, was used to obtain the energy barrier [47]. The different charge densities were calculated by subtracting the charge density of the substrate and $PhNO_2$ from the $PhNO_2$-absorbed system.

To simplify the calculation for hydrogenation of nitrobenzene, the hydrogen atoms and the water molecules were excluded from the slab model calculations. According to Mondal's scheme [48], the reaction energies were calculated using the following formula:

$$\Delta E_{\text{reaction}} = \left[E_{\text{product}}{}^{*} + n_{\text{water}} \times \left(E_{\text{water}} - E_{\text{b\_water}}\right)\right] - \left[E_{\text{reactant}}{}^{*} + n_{\text{H}} \times \left(E_{\text{H}} - E_{\text{b\_H}}\right)\right],$$

where $E_{\text{reactant}}{}^{*}$ means the total energy of the system in which the reactant is bound to the slab; $E_{\text{product}}{}^{*}$ means the total energy of the system in which the product is bound to the slab while the generated water molecule does not exist; n_{water} is the number of water molecules dissociating from the reactant and n_{H} is the number of hydrogen atoms; E_{water} and E_{H} are the energies of an isolated water molecule and hydrogen atom, respectively; $E_{\text{b\_water}}$ and $E_{\text{b\_H}}$ represent the binding energies of a water molecule (a hydrogen atom) on a clean surface.

RESULTS AND DISCUSSION

The preparation of the Fe_1/N-C sample included the following three-step procedures. Firstly, g-C_3N_4 was prepared by the pyrolyzation of dicyandiamide. Then, a thin layer of polydopamine (PDA) doped by $Fe(acac)_3$ was coated on g-C_3N_4 surface to form the $Fe(acac)_3$-PDA@g-C_3N_4 composite. Finally, the above composite was pyrolyzed to form the final Fe_1/N-C sample. The prepared g-C_3N_4 exhibited nanosheet morphology (Fig. S1). The XRD pattern shows that the obtained sample has the typical g-C_3N_4 crystal pattern (Fig. S2). The g-C_3N_4 was crucial for the preparation of Fe_1/N-C because it was used as both a soft template to obtain the layer structure and a nitrogen source to obtain high-content-nitrogen-doped carbon. TEM image shows that the Fe_1/N-C sample has a nanosheet morphology, and no obvious Fe-containing nanoparticles are observed (Fig. 1a). And XRD pattern shows that the spectrum of Fe_1/N-C has one broad diffraction peak, with 2θ in the range of 15°–35°, which could be assigned to the diffraction character of (002) of graphitic carbon and is similar to the N-C and Fe nanoparticles/N-C (Figs S3–S5). Moreover, no diffraction peak assigned to metallic Fe was found, eliminating the existence of Fe-containing crystalline species. Besides, no Fe-containing nanoparticle was found in the HAADF-STEM image (Fig. 1b). Meanwhile, the energy-dispersive X-ray (EDX) spectroscopy reveals that Fe and N atoms are uniformly distributed in the carbon nanosheets (Fig. 1c), and the nitrogen content is up to about 4.7 wt% (Fig. S6 and Table S1). Furthermore, the ICP-OES shows that the Fe content is as high as 2.1 wt%. Nitrogen adsorption-desorption isotherms show that the Brunauer-Emmett-Teller (BET) surface areas of N/C, Fe_1/N-C, and Fe nano-

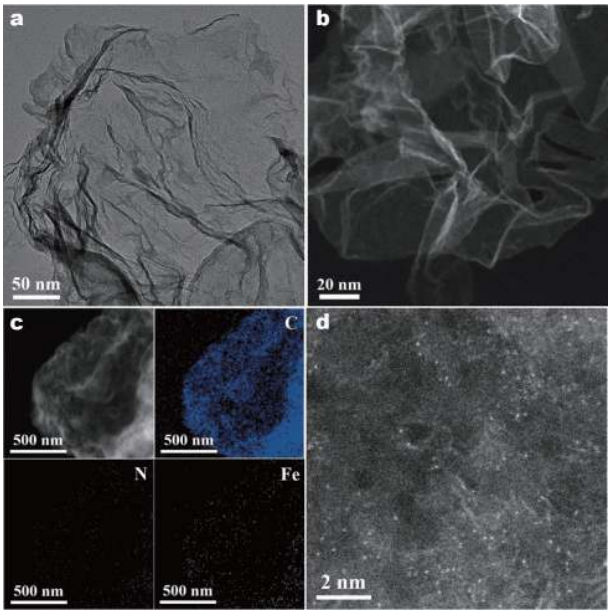

Figure 1 (a, b) TEM and STEM images of Fe_1/N-C. (c) EDX mapping distributions of C, N, and Fe, respectively. (d) AC STEM image of Fe_1/N-C.

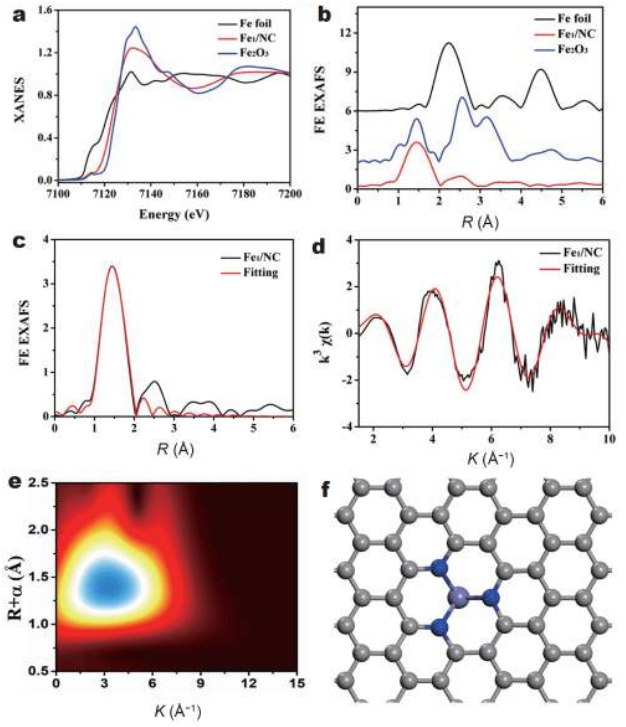

Figure 2 (a, b) XANES and FT EXAFS spectra at the Fe K-edge of Fe_1/N-C, Fe foil, and Fe_2O_3. (c, d) The fittings of the EXAFS spectra of Fe_1/N-C at R- and K-spaces, respectively. (e) WT EXAFS spectra of Fe_1/N-C. (f) The structural model of Fe_1/N-C, C (gray), N (blue), and Fe (purple).

particles/N-C are approximately 338, 311, and 297 $m^2 g^{-1}$, respectively. And the average pore diameters of N/C, Fe_1/N-C, and Fe nanoparticles/N-C are 2–3 nm (Figs S7–S12). The AC HAADF-STEM image reveals that many single bright dots are homogeneously distributed on the support, which could be assigned to the Fe atoms (Fig. 1d). Besides, no Fe-containing nanocluster was found, further confirming that the Fe species is the single-atom state.

The detailed charge state and coordinate structure of Fe atom were further determined by the XAFS spectroscopy. The Fe K-edge X-ray absorption near-edge structure (XANES) spectra show that the absorption profile of Fe_1/N-C was significantly different from that of Fe foil and Fe_2O_3, demonstrating the unique structure of Fe_1/N-C (Fig. 2a). Moreover, the absorption edge and white line intensity of Fe_1/N-C were located between the Fe foil and Fe_2O_3, indicating that the valence state of Fe was between 0 and 3. To reveal the coordinate structure of Fe_1/N-C, the Fourier-transformed k^3-weighted EXAFS (FT EXAFS) measurement was further performed. Only one prominent peak at 1.4 Å was observed in the FT EXAFS spectrum of Fe_1/N-C, which could be ascribed to the Fe–N/C contributions. Besides, no evident peak at around 2.4 Å corresponding to the Fe–Fe contribution was observed, demonstrating that the Fe_1/N-C sample contained only single-atom Fe (Fig. 2b). Moreover, wavelet transform (WT) EXAFS analysis results show only one intensity maximum at 3.2 $Å^{-1}$ in K-space and 1.4 Å in R-space in the WT EXAFS spectrum of Fe_1/N-C, which is corresponding to the Fe–N/C bond and further indicates that the Fe species in Fe_1/N-C exists as single-atom Fe (Fig. 2e and Figs S13, S14). Therefore, it can be evidenced that the Fe exists as single-atoms in Fe_1/N-C by the AC HAADF-STEM and EXAFS analysis. EXAFS fitting was further performed to obtain the detailed structure configuration of the Fe atom. According to the fitting results, the coordination numbers of Fe–C/N within Fe_1/N-C are approximate 3.1 and the average bond length of Fe–N is 1.83 Å (Fig. 2c, d, and Fig. S15, Table S2). The structure of Fe_1/N-C was further confirmed by DFT calculations (Fig. 2f). Herein, every Fe atom was anchored by three N atoms and the Fe–N bond length was calculated to be 1.82 Å by the DFT calculations, which is in good agreement with the experimental results from the XAFS spectra.

Next, we chose the selective hydrogenation and transfer hydrogenation of nitrobenzene to investigate the performance of the Fe_1/N-C sample. By optimizing the reaction

conditions, the Fe_1/N-C catalyst showed superior properties for the selective hydrogenation and transfer hydrogenation with hydrogen molecule and isopropanol as the hydrogen source, respectively. As shown in Table 1, >99% conversion and >99% selectivity for the selective hydrogenation of nitrobenzene to aniline were achieved at 160°C. When the temperature rose to 220°C, the conversion of >99% and selectivity of >99% for the transfer hydrogenation of nitrobenzene to aniline were also achieved. Therefore, the superior performances of the selective hydrogenation and transfer hydrogenation could be achieved by the Fe_1/N-C catalyst, which was one of the best results for the selective hydrogenation and transfer hydrogenation of nitrobenzene catalyzed by Fe-based catalysts (Table S3). However, the N-C itself was reactively inert for hydrogenation and transfer hydrogenation of nitrobenzene under the same condition. When Fe nanoparticles/N-C (Fig. S16) was used as catalyst, only trace product was obtained, indicating that the superior performance of the single-atom Fe (Table 1). Moreover, the Fe_1/N-C catalyst showed robust recycling capability in both selective hydrogenation and transfer hydrogenation (Figs S17 and S18). HAADF-STEM images and XRD patterns demonstrate that the morphology and structure of Fe_1/N-C did not change and no Fe nanoparticles or nanoclusters were obsevered after the reactions, which further demonstrates the robust stability of the Fe_1/N-C catalyst (Figs S19 and S20). To verify the universal catalytic performace of Fe_1/N-C, we explored the hydrogenation of several other nitroarene derivatives, including 4-nitrobenzene, 4-nitrotoluene, 4-nitrochlorobenzene, and 4-bromonitrobenzene. The results showed that Fe_1/N-C exhibited excellent peformance for all corresponding anilines (Table 1).

In order to understand the excellent catalytic performance of Fe_1/N-C in the hydrogenation of nitrobenzene to aniline, the reaction energies on Fe_1/N-C and Fe (100), which is the commonly active surface for the Fe-based catalyst [49–51], were explored by DFT calculations. In addition, Fe (100) facet was selected for our calculations because the Fe (100) facet is often used as the representative facet of Fe nanoparticles to discuss calculation-related issues qualitatively [52–54]. At the same time, the formation energies of the Fe (100), (111), and (211) planes were calculated (Fig. S21). The results showed that the Fe (100) plane is more stable. Firstly, for the adsorption of nitrobenzene, the configurations of adsorbate on Fe_1/N-C and Fe (100) are parallel to the catalyst sur-

Table 1 Selective hydrogenation and transfer hydrogenation of nitrobenzenes to anilines at different temperatures[a]

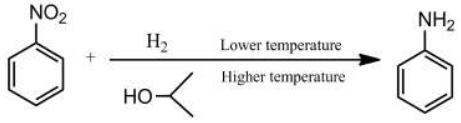

Catalyst	Reactant	Temperature (°C)	Hydrogen source	Conversion (%)	Selectivity (%)	Yeild (%)
Fe_1/N-C	Nitrobenzene	120	H_2	N.R.	–	–
Fe_1/N-C	Nitrobenzene	140	H_2	14	>99	14
Fe_1/N-C	Nitrobenzene	160	H_2	>99	>99	>99
Fe_1/N-C	4-Nitrophenol	160	H_2	>99	>99	>99
Fe_1/N-C	4-Nitrotoluene	160	H_2	92	>99	92
Fe_1/N-C	4-Nitrochlorobenzene	160	H_2	94	>99	94
Fe_1/N-C	4-Bromonitrobenzene	160	H_2	92	>99	92
N-C	Nitrobenzene	160	H_2	N.R.	–	–
Fe nano particle/N-C	Nitrobenzene	160	H_2	Trace	–	–
Fe_1/N-C	Nitrobenzene	160	Isopropanol	N.R.	–	–
Fe_1/N-C	Nitrobenzene	180	Isopropanol	21	>99	21
Fe_1/N-C	Nitrobenzene	200	Isopropanol	45	>99	45
Fe_1/N-C	Nitrobenzene	220	Isopropanol	>99	>99	>99
N-C	Nitrobenzene	220	Isopropanol	N.R.	–	–
Fe nano particle/N-C	Nitrobenzene	220	Isopropanol	Trace	–	–

a) Time: 5 h; solvent: isopropanol; H_2: 5 bar.

faces. This parallel adsorption mode of nitrobenzene on the metal surface, rather than the vertical one, is consistent with previous studies [55,56]. In addition, we calculated the charge density difference of nitrobenzene on the surface of different catalysts. The results showed that for Fe surface, both the benzene ring and the NO_2 group in the molecule had electron exchange with the catalyst surface; while on the Fe_1/N-C surface, the electron exchange was mainly concentrated on the NO_2 group, and the electron exchange effect was stronger. This indicates that Fe_1/N-C can activate nitrobenzene more effectively.

According to the previous reports, the hydrogenation reduction of nitrobenzene to aniline follows the direct reaction pathway, namely $PhNO_2^* \rightarrow PhNOOH^* \rightarrow PhNO^* \rightarrow PhNOH^* (PhNHO^*) \rightarrow PhNHOH^* \rightarrow PhNH^* \rightarrow PhNH_2^*$ [57,58]. The full reaction energy profiles along the pathway are collected in Fig. 3, and the structure diagram of each intermediate is shown in Tables S4–S7. In the hydrogenation reaction, the hydrogen atom and the oxygen atom of $PhNO_2$ are firstly combined to obtain the PhNOOH intermediate, then reduced to PhNO intermediate (−2.30 eV on Fe_1/N-C and +0.25 eV on Fe surface). Then, the H atom can attack the O atom or N atom of the PhNO intermediate, forming PhNOH or PhNHO intermediates, respectively (−0.12/−0.64 eV on Fe_1/N-C and −0.26/+1.46 eV on Fe surface). In the next step, the H atom interacts with a PhNOH or PhNHO intermediate to form a PhNHOH intermediate (−2.09/−1.57 eV on Fe_1/N-C and +1.73/+0.02 eV on Fe surface). Finally, the hydrogen atom combines with PhNH to form aniline. From the above analysis, we can see that for the hydrogenation of nitrobenzene, the full pathway on FeNC catalyst is an exothermic process, and there is no reaction energy barrier; for Fe surface, the reaction energy barrier for the hydrogenation process is +1.45 eV. Therefore, the reactivity of Fe_1/N-C is significantly higher than that of Fe nanoparticles.

To further reveal the excellent performance of Fe_1/N-C for the transfer hydrogenation of nitrobenzene to aniline with the isopropanol as the hydrogen donor, we further calculated the dehydrogenation reaction barrier of isopropanol on Fe_1/N-C and Fe surface. The reaction barrier and the structure of transition state are shown in Fig. 4. The calculation results show that the energy barrier for isopropanol dehydrogenation is 1.88 eV, which could be

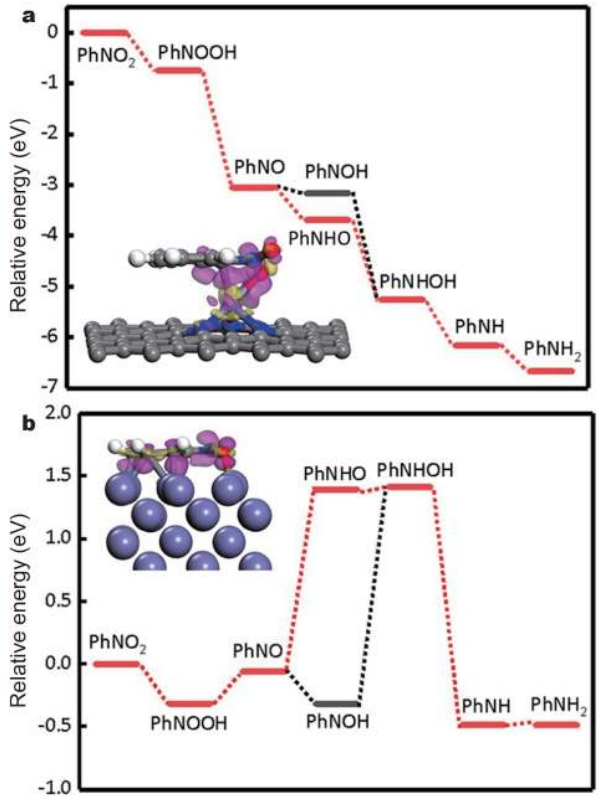

Figure 3 Reaction energy profiles of nitrobenzene hydrogenation and charge density difference of $PhNO_2$ on (a) Fe_1/N-C and (b) Fe (100). The yellow and purple regions represent the deletion and accumulation of electrons, respectively.

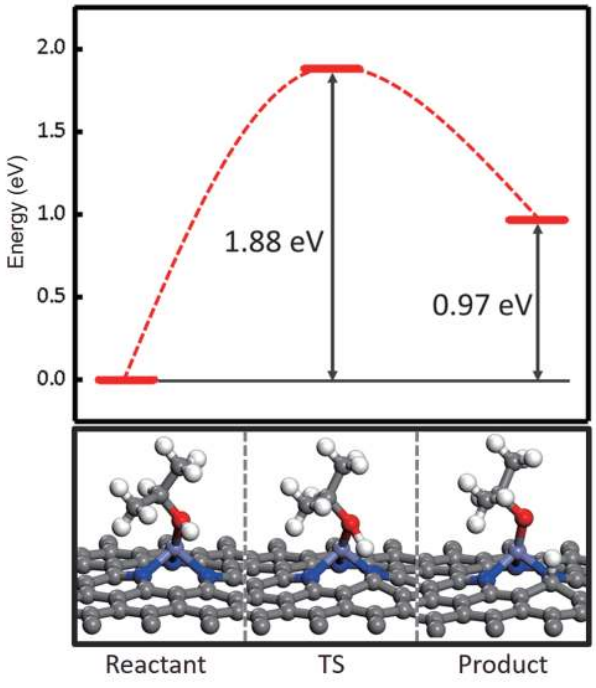

Figure 4 The reaction barrier for the dehydrogenation of isopropanol on Fe_1/N-C.

overcome by the increasing reaction temperature, consistent with the experimental results.

CONCLUSIONS

In summary, we have successfully synthesized the single-atom Fe supported by nitrogen-doped carbon. The as-prepared Fe_1/N-C sample possessed the Fe_1N_3 structure which showed superior performances in both the hydrogenation and transfer hydrogenation of nitrobenzene in isopropanol solution. DFT showed that the unique catalytic activity of the Fe_1/N-C originated from the fact that the reactant could be effectively activated. Moreover, the excellent performance of Fe_1/N-C catalyst for transfer hydrogenation can be attributed to that the dehydrogenation reaction energy barrier of isopropanol can be overcome by elevated temperature.

Received 3 June 2020; accepted 26 June 2020; published online 15 October 2020

1 Downing RS, Kunkeler PJ, van Bekkum H. Catalytic syntheses of aromatic amines. Catal Today, 1997, 37: 121–136
2 Blaser HU, Steiner H, Studer M. Selective catalytic hydrogenation of functionalized nitroarenes: An update. ChemCatChem, 2009, 1: 210–221
3 Corma A, Serna P. Chemoselective hydrogenation of nitro compounds with supported gold catalysts. Science, 2006, 313: 332–334
4 Wienhofer G, Sorribes I, Boddien A, *et al.* General and selective iron-catalyzed transfer hydrogenation of nitroarenes without base. J Am Chem Soc, 2011, 133: 12875–12879
5 Jagadeesh RV, Surkus AE, Junge H, *et al.* Nanoscale Fe_2O_3-based catalysts for selective hydrogenation of nitroarenes to anilines. Science, 2013, 342: 1073–1076
6 Westerhaus FA, Jagadeesh RV, Wienhöfer G, *et al.* Heterogenized cobalt oxide catalysts for nitroarene reduction by pyrolysis of molecularly defined complexes. Nat Chem, 2013, 5: 537–543
7 Li H, Cao C, Liu J, *et al.* Cobalt single atoms anchored on N-doped ultrathin carbon nanosheets for selective transfer hydrogenation of nitroarenes. Sci China Mater, 2019, 62: 1306–1314
8 You Y, Huang H, Mao K, *et al.* Tandem nanocatalyst design: Putting two step-reaction sites into one location towards enhanced hydrogen transfer reactions. Sci China Mater, 2019, 62: 1297–1305
9 Lin L, Yao S, Gao R, *et al.* A highly CO-tolerant atomically dispersed Pt catalyst for chemoselective hydrogenation. Nat Nanotechnol, 2019, 14: 354–361
10 Li X, Wang Z, Mao S, *et al.* Insight into the role of additives in catalytic synthesis of cyclohexylamine from nitrobenzene. Chin J Chem, 2018, 36: 1191–1196
11 Chen Y, Wang Z, Mao S, *et al.* Rational design of hydrogenation catalysts using nitrogen-doped porous carbon. Chin J Catal, 2019, 40: 971–979
12 Shimizu K, Miyamoto Y, Satsuma A. Size- and support-dependent silver cluster catalysis for chemoselective hydrogenation of nitroaromatics. J Catal, 2010, 270: 86–94
13 Jagadeesh RV, Wienhöfer G, Westerhaus FA, *et al.* Efficient and highly selective iron-catalyzed reduction of nitroarenes. Chem Commun, 2011, 47: 10972–10974
14 Nie R, Wang J, Wang L, *et al.* Platinum supported on reduced graphene oxide as a catalyst for hydrogenation of nitroarenes. Carbon, 2012, 50: 586–596
15 Zhang S, Chang CR, Huang ZQ, *et al.* High catalytic activity and chemoselectivity of sub-nanometric Pd clusters on porous nanorods of CeO_2 for hydrogenation of nitroarenes. J Am Chem Soc, 2016, 138: 2629–2637
16 Fürstner A, Leitner A, Méndez M, *et al.* Iron-catalyzed cross-coupling reactions. J Am Chem Soc, 2002, 124: 13856–13863
17 Bolm C, Legros J, Le Paih J, *et al.* Iron-catalyzed reactions in organic synthesis. Chem Rev, 2004, 104: 6217–6254
18 Morris RH. Asymmetric hydrogenation, transfer hydrogenation and hydrosilylation of ketones catalyzed by iron complexes. Chem Soc Rev, 2009, 38: 2282–2291
19 Yang M, Allard LF, Flytzani-Stephanopoulos M. Atomically dispersed Au–$(OH)_x$ species bound on titania catalyze the low-temperature water-gas shift reaction. J Am Chem Soc, 2013, 135: 3768–3771
20 Liu J, Lucci FR, Yang M, *et al.* Tackling CO poisoning with single-atom alloy catalysts. J Am Chem Soc, 2016, 138: 6396–6399
21 Chen H, He S, Cao X, *et al.* Ru-cluster-modified Ni surface defects toward selective bond breaking between C–O and C–C. Chem Mater, 2016, 28: 4751–4761
22 Zhang H, Wei J, Dong J, *et al.* Efficient visible-light-driven carbon dioxide reduction by a single-atom implanted metal-organic framework. Angew Chem Int Ed, 2016, 55: 14310–14314
23 Malta G, Kondrat SA, Freakley SJ, *et al.* Identification of single-site gold catalysis in acetylene hydrochlorination. Science, 2017, 355: 1399–1403
24 Huang F, Deng Y, Chen Y, *et al.* Atomically dispersed Pd on nanodiamond/graphene hybrid for selective hydrogenation of acetylene. J Am Chem Soc, 2018, 140: 13142–13146
25 Qin R, Liu P, Fu G, *et al.* Strategies for stabilizing atomically dispersed metal catalysts. Small Methods, 2018, 2: 1700286
26 Li H, Wang L, Dai Y, *et al.* Synergetic interaction between neighbouring platinum monomers in CO_2 hydrogenation. Nat Nanotech, 2018, 13: 411–417
27 Abdel-Mageed AM, Rungtaweevoranit B, Parlinska-Wojtan M, *et al.* Highly active and stable single-atom Cu catalysts supported by a metal-organic framework. J Am Chem Soc, 2019, 141: 5201–5210
28 Cao L, Liu W, Luo Q, *et al.* Atomically dispersed iron hydroxide anchored on Pt for preferential oxidation of CO in H_2. Nature, 2019, 565: 631–635
29 Sun T, Xu L, Wang D, *et al.* Metal organic frameworks derived single atom catalysts for electrocatalytic energy conversion. Nano Res, 2019, 12: 2067–2080
30 Lee BH, Park S, Kim M, *et al.* Reversible and cooperative photoactivation of single-atom Cu/TiO_2 photocatalysts. Nat Mater, 2019, 18: 620–626
31 Yan J, Kong L, Ji Y, *et al.* Single atom tungsten doped ultrathin α-$Ni(OH)_2$ for enhanced electrocatalytic water oxidation. Nat Commun, 2019, 10: 2149
32 Xi W, Wang K, Shen Y, *et al.* Dynamic co-catalysis of Au single atoms and nanoporous Au for methane pyrolysis. Nat Commun, 2020, 11: 1919
33 Xu Q, Guo CX, Tian S, *et al.* Coordination structure dominated performance of single-atomic Pt catalyst for anti-Markovnikov hydroboration of alkenes. Sci China Mater, 2020, 63: 972–981
34 Gong YN, Jiao L, Qian Y, *et al.* Regulating the coordination en-

vironment of MOF-templated single-atom nickel electrocatalysts for boosting CO_2 reduction. Angew Chem Int Ed, 2020, 59: 2705–2709
35 Li X, Rong H, Zhang J, *et al.* Modulating the local coordination environment of single-atom catalysts for enhanced catalytic performance. Nano Res, 2020, 13: 1842–1855
36 Zhuang Z, Kang Q, Wang D, *et al.* Single-atom catalysis enables long-life, high-energy lithium-sulfur batteries. Nano Res, 2020, 13: 1856–1866
37 Deng D, Chen X, Yu L, *et al.* A single iron site confined in a graphene matrix for the catalytic oxidation of benzene at room temperature. Sci Adv, 2015, 1: e1500462
38 Wu P, Du P, Zhang H, *et al.* Graphyne-supported single Fe atom catalysts for CO oxidation. Phys Chem Chem Phys, 2015, 17: 1441–1449
39 Chen P, Zhou T, Xing L, *et al.* Atomically dispersed iron-nitrogen species as electrocatalysts for bifunctional oxygen evolution and reduction reactions. Angew Chem Int Ed, 2017, 56: 610–614
40 Liu W, Zhang L, Liu X, *et al.* Discriminating catalytically active FeN_x species of atomically dispersed Fe–N–C catalyst for selective oxidation of the C–H bond. J Am Chem Soc, 2017, 139: 10790–10798
41 Fei H, Dong J, Feng Y, *et al.* General synthesis and definitive structural identification of MN_4C_4 single-atom catalysts with tunable electrocatalytic activities. Nat Catal, 2018, 1: 63–72
42 Yang L, Cheng D, Xu H, *et al.* Unveiling the high-activity origin of single-atom iron catalysts for oxygen reduction reaction. Proc Natl Acad Sci USA, 2018, 115: 6626–6631
43 Wan X, Liu X, Li Y, *et al.* Fe–N–C electrocatalyst with dense active sites and efficient mass transport for high-performance proton exchange membrane fuel cells. Nat Catal, 2019, 2: 259–268
44 Delley B. From molecules to solids with the $DMol^3$ approach. J Chem Phys, 2000, 113: 7756–7764
45 Runge E, Gross EKU. Density-functional theory for time-dependent systems. Phys Rev Lett, 1984, 52: 997–1000
46 Ernzerhof M, Scuseria GE. Assessment of the Perdew-Burke-Ernzerhof exchange-correlation functional. J Chem Phys, 1999, 110: 5029–5036
47 Halgren TA, Lipscomb WN. The synchronous-transit method for determining reaction pathways and locating molecular transition states. Chem Phys Lett, 1977, 49: 225–232
48 Mondal J, Kundu SK, Hung Ng WK, *et al.* Fabrication of ruthenium nanoparticles in porous organic polymers: Towards advanced heterogeneous catalytic nanoreactors. Chem Eur J, 2015, 21: 19016–19027
49 Ertl G, Grunze M, Weiss M. Chemisorption of N_2 on an Fe(100) surface. J Vac Sci Technol, 1976, 13: 314–317
50 Benziger J. Reactions and reaction intermediates on iron surfaces I. Methanol, ethanol, and isopropanol on Fe(100). J Catal, 1980, 65: 36–48
51 Benziger J, Madix RJ. The effects of carbon, oxygen, sulfur and potassium adlayers on CO and H_2 adsorption on Fe(100). Surf Sci, 1980, 94: 119–153
52 Luo Q, Pan Y, Guo P, *et al.* First-principles calculation of adsorption of shale gas on $CaCO_3$ (100) surfaces. J Appl Biomater Funct Mater, 2017, 15: 45–51
53 Saraireh SA, Altarawneh M, Tarawneh MA. Adsorption and dissociation of the methanethiol (CH_3SH) molecule on the Fe(100) surface. Surf Interface Anal, 2019, 52: 156–166
54 Hensley AJR, Collinge G, Wang Y, *et al.* Coverage-dependent adsorption of hydrogen on Fe(100): Determining catalytically relevant surface structures *via* lattice gas models. J Phys Chem C, 2020, 124: 7254–7266
55 Jenkins SJ. Aromatic adsorption on metals *via* first-principles density functional theory. Proc R Soc A, 2009, 465: 2949–2976
56 Honkela ML, Björk J, Persson M. Computational study of the adsorption and dissociation of phenol on Pt and Rh surfaces. Phys Chem Chem Phys, 2012, 14: 5849–5854
57 Mahata A, Rai RK, Choudhuri I, *et al.* Direct *vs.* indirect pathway for nitrobenzene reduction reaction on a Ni catalyst surface: A density functional study. Phys Chem Chem Phys, 2014, 16: 26365–26374
58 Morrissey C, He H. Silicene catalyzed reduction of nitrobenzene to aniline: A mechanistic study. Chem Phys Lett, 2018, 695: 228–234

Acknowledgements This work was supported by the National Key R&D Program of China (2018YFA0702003), the National Natural Science Foundation of China (21890383, 21671117, 21871159 and 21901135), and the Science and Technology Key Project of Guangdong Province of China (2020B010188002). We thank the 1W1B station in Beijing Synchrotron Radiation Facility.

Author contributions Tian S designed and performed the experiments, and analyzed the data; Hu M and He J conducted the density functional theory calculations; Xu Q and Zhu Y assisted to carry out the experiments; Gong W, Chen C, and Zhao H designed and performed the catalytic experiment; Chen W and Yang J helped with XAFS characterization and the corresponding data analysis; Liu Q assisted to analyze the data; Wang D and Li Y conceived the research project, and analyzed the results. All authors contributed to the general discussion and writing the paper.

Conflict of interest The authors declare that they have no conflict of interest.

Supplementary information Supporting data are available in the online version of the paper.

Shubo Tian received his BSc (2013), MSc (2016), and PhD (2019) degrees from Hebei Normal University, University of the Chinese Academy of Sciences, and Tsinghua University, respectively. He is currently a postdoctor in the National University of Singapore. His research interests are focused on the syntheses and applications of isolated single-atom-site and cluster catalysts.

Min Hu received her BSc (2018) degree from Ludong University. She is currently studying for a master's degree at the Institute for New Energy Materials and Low-Carbon Technology, Tianjin University of Technology. Her main research directions are first-principles and molecular dynamics simulations.

Qi Xu received his BSc degree from the University of Science and Technology of China in 2017. Now, he is a PhD student under the supervision of Prof. Dingsheng Wang at Tsinghua University. His research interests mainly focus on the design and fabrication of single-atomic catalysts for heterogeneous catalysis.

Dingsheng Wang received his BSc degree from the Department of Chemistry and Physics, University of Science and Technology of China in 2004, and his PhD degree from the Department of Chemistry, Tsinghua University in 2009, under the supervision of Prof. Yadong Li. He did his postdoctoral research at the Department of Physics, Tsinghua University, with Prof. Shoushan Fan. He joined the faculty of the Department of Chemistry, Tsinghua University in 2012.

Fe_1N_3结构单原子Fe催化剂在硝基苯加氢和转移加氢中的优异性能

田书博[1†], 胡敏[2†], 徐琪[1†], 龚万兵[3], 陈文星[4], 杨嘉睿[1], 朱有奇[4], 陈春[3], 何佳[2], 刘强[1], 赵惠军[3], 王定胜[1*], 李亚栋[1]

摘要 设计性能优异的硝基化合物选择性加氢或转移加氢生成胺类的非贵金属多相催化剂具有重要的意义，但又具有很大的挑战性. 本文报道了氮掺杂碳负载的单原子Fe催化剂(Fe_1/N-C). 通过调控温度，Fe_1/N-C催化剂对硝基苯的选择性加氢和转移加氢均具有良好的催化性能. DFT计算表明，Fe_1/N-C在较低温度下能够很好地活化反应物和中间体，因此具有较高的选择性加氢活性. 此外，Fe_1/N-C在较高温度下可以克服异丙醇脱氢反应的能量障碍，因此具有很好的转移加氢性能.